Microchemical Journal 117 (2014) 202–213

Contents lists available at ScienceDirect

Microchemical Journal

journal homepage: www.elsevier.com/locate/microc

# Source identification of sea surface oil with geochemical data in Cantarell, Mexico ☆

Caroline C. Texeira [a], Celeste Y. Santos Siqueira [a,*], Francisco R. Aquino Neto [a], Fernando P. Miranda [b], José R. Cerqueira [b], Adriano O. Vasconcelos [c], Luis Landau [c], Miguel Herrera [d], Karen Bannermaman [e]

[a] Universidade Federal do Rio de Janeiro, Instituto de Química, LADETEC, Ilha do Fundão, Rio de Janeiro 21949, Brazil
[b] PETROBRAS Research and Development Center (PETROBRAS/CENPES), Av. Horácio Macedo, No. 950, Cidade Universitária, Ilha do Fundão, 21491-915 Rio de Janeiro, Brazil
[c] Universidade Federal do Rio de Janeiro, LAMCE/COPPE, P.O. Box 68552, Ilha do Fundão, Rio de Janeiro 21949, Brazil
[d] PEMEX Exploración y Producción, Región Marina Norest (PEP/RMNE), Estudios Ambientales, Call 25, No. 48, Col. Guadalupe. Cd Del Carmen, Campeche C.P. 24130, Mexico
[e] MacDonald, Dettwiler and Associates Ltd., 13800 Commerce Parkway, Richmond, British Columbia V6V 2J3, Canada

ARTICLE INFO

*Article history:*
Received 19 December 2013
Received in revised form 24 April 2014
Accepted 27 June 2014
Available online 5 July 2014

*Keywords:*
Seep
Oil
Biomarkers
Diamondoids
Mexico
Gas chromatography
GC-MS

ABSTRACT

The Gulf of Mexico is one of the world's largest petroleum regions. Cantarell is an important oil field located in the Akal Pillar province. This region is characterized by several oil seeps. However, there is no consensus on the Cantarell oil seep subsurface provenance. Surface oil samples (seepage) and subsurface oil samples (reservoirs) from the Akal Pillar province were analyzed using gas chromatography with a flame ionization detector (GC-FID) and gas chromatography with a mass spectrometry detector (GC-MS). The data obtained were used to identify and characterize biomarker and diamondoid distributions. Multivariate statistical analyses of geochemical results were made to identify the Cantarell oil seep origin. Geochemical analysis showed small differences between the results which could help the correlation studies between the samples. Cluster analysis indicated a good correlation of the seepage samples with a unique subsurface oil sample, CAN8, from the reservoir in the Paleocene/Cretaceous breccia.



## 1. Introduction

Large and numerous hydrocarbon seeps have been known to pre-Colombian populations of southern Gulf of Mexico coastal areas for many centuries [1,2]. They referred to them as *chapopoteras* in their native dialect. Onshore oil seeps also attracted the attention of entrepreneurs in the late 19th century with initial production activities west of Tampico. Hydrocarbon exploration and production efforts in southern Gulf of Mexico moved offshore in the 20th century and culminated in 1976 with the giant Cantarell oil field discovery in the Bay of Campeche [2,3]. Mexican exploration activities in this oceanic region began soon after a fisherman, Mr. Cantarell, reported seepage phenomena in the Campeche Bay. The oil fields complex discovered beneath the seeps was subsequently named after him.

Nowadays, PEMEX Exploration and Production (PEP) shares the operational marine area, where vessel related to important fisheries or industrial transport traffic through delicate ecosystems, making it highly sensitive to the presence of oil [4]. Therefore, sea surface oil slicks or deposits on the seashore are immediately related to PEP activities, which generate claims and social pressures with economic and public image impacts [5]. To establish proper environmental management practices, PEP is using spaceborne radar remote sensing together with high resolution geochemistry technology to characterize oil seeps in the Cantarell Complex area.

As part of this research effort, 21 oil samples were collected between 2003 and 2007 from the Cantarell seep as well as different platforms for further geochemical analysis. This procedure was also carried out from 2007 to 2010 to better understand the temporal and spatial distribution of natural seepage phenomena in the Campeche Bay. This study describes methodological aspects and the results achieved in comparing the different samples' geochemical characteristics to determine the

☆ Paper presented at the Brazilian Congress on Analytical Chemistry.

* Corresponding author at: Instituto de Química da Universidade Federal do Rio de Janeiro (IQ/UFRJ). Avenida Athos da Silveira Ramos, 149, Centro de Tecnologia (CT), bloco A, sala 607, Ilha do Fundão, Cidade Universitária, Rio de Janeiro, RJ 21941-909, Brazil. Tel./fax: +55 21 2260 3967.
*E-mail address:* celesteyara@iq.ufrj.br (C.Y. Santos Siqueira).

http://dx.doi.org/10.1016/j.microc.2014.06.025
0026-265X/

Cantarell oil seep subsurface provenance. This approach can be used in the future as a complementary tool for an operational multiyear monitoring program in southern Gulf of Mexico.

Each oil sample contains a unique distribution of compounds considered as a fingerprint and oil geochemistry is a fundamental issue for any regional exploration for new frontiers and production programs. It can

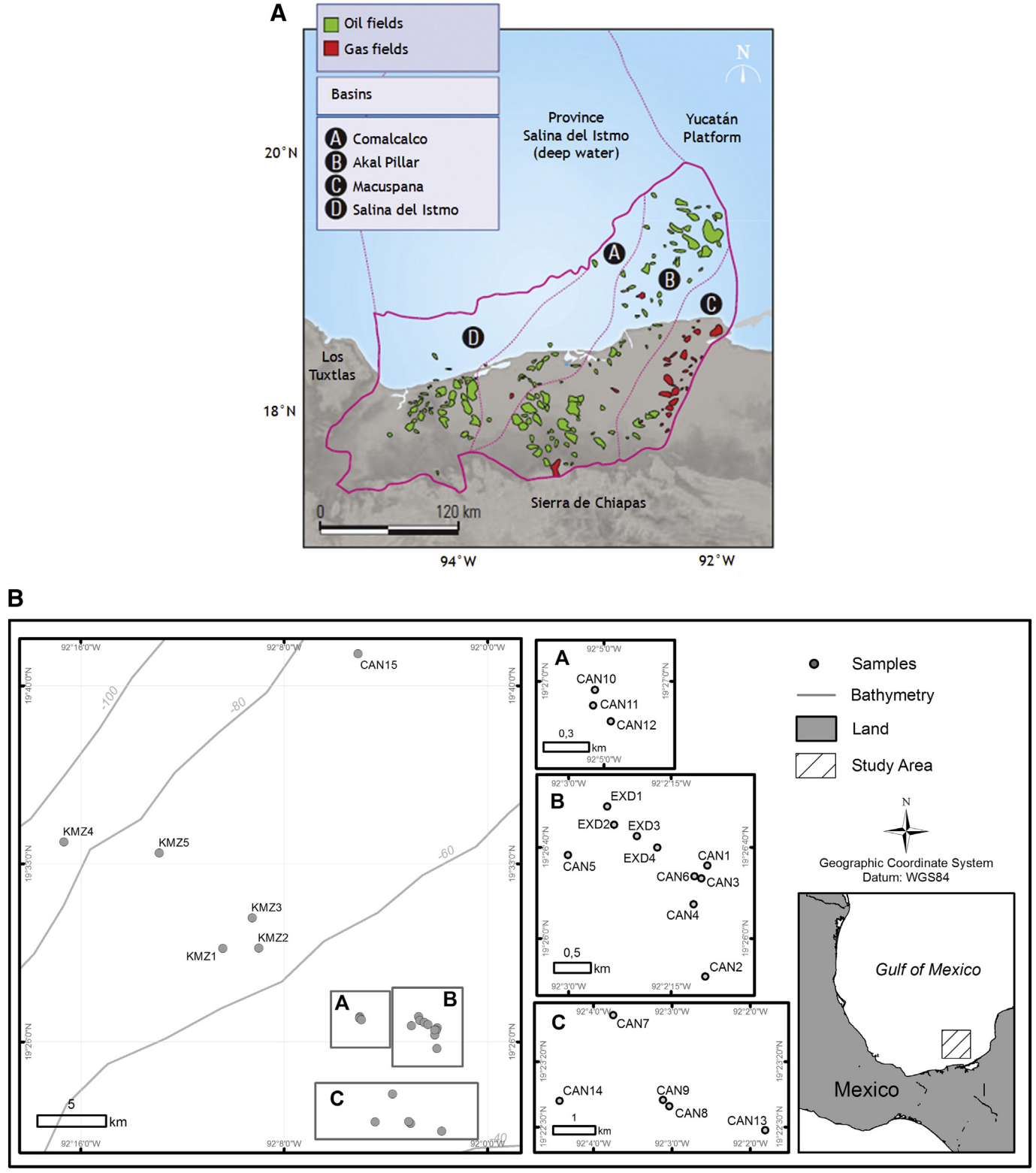


**Fig. 1.** A: Oil and gas field locations in the Akal Pillar province, Gulf of Mexico (adapted from Miranda et al., 2004). B: Map of Gulf of Mexico identifying the localization of the samples. C: Map of Gulf of Mexico identifying the ocean currents (adapted from http://flowergarden.noaa.gov/about/naturalsetting.html#currents) [6]. D: Map of Gulf of Mexico identifying structural geologic of the sampling site.

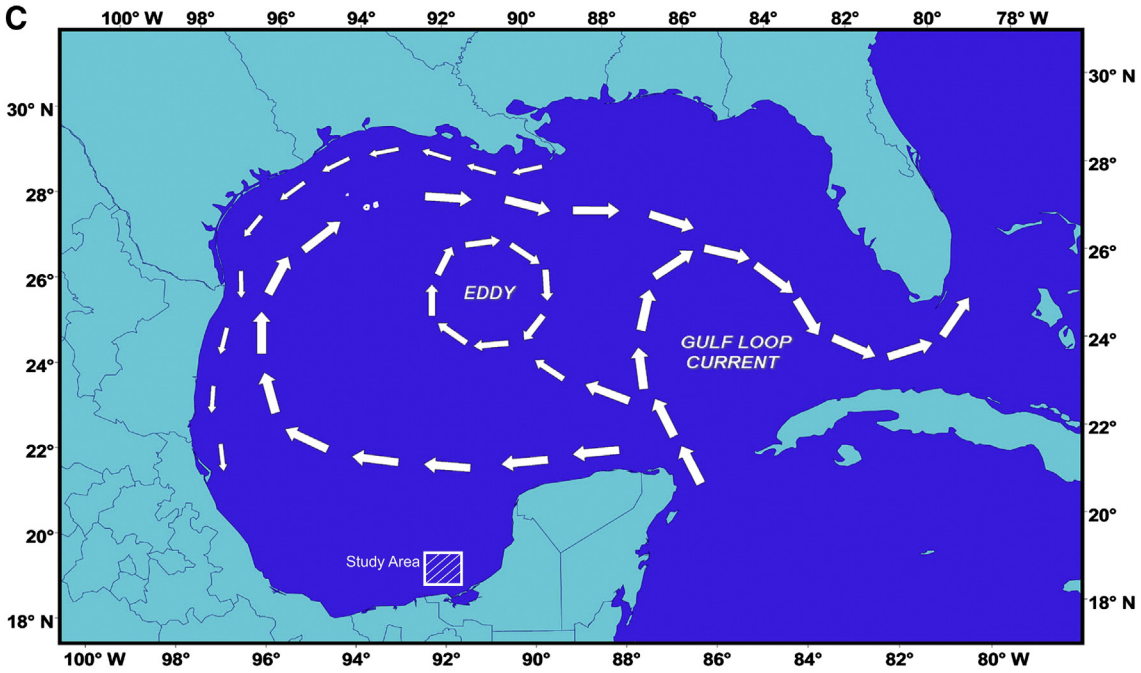


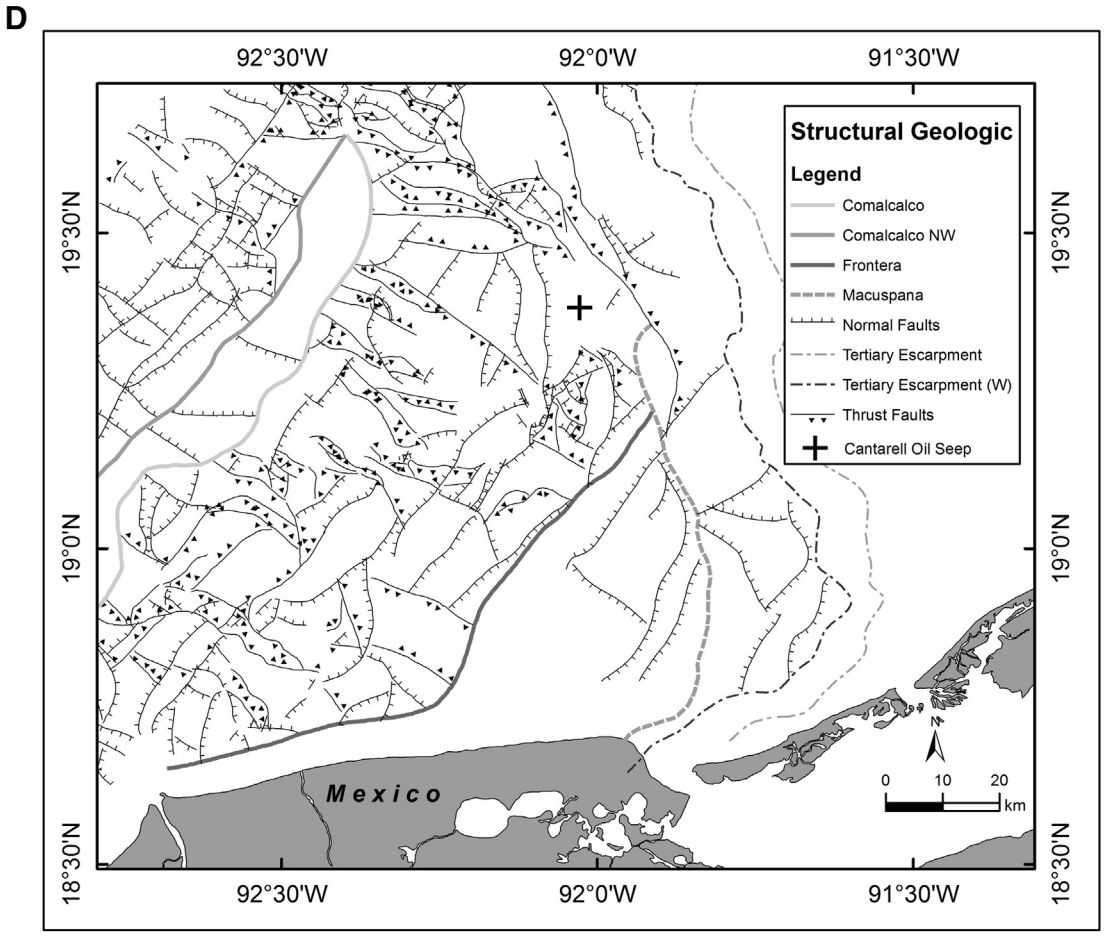


**Fig. 1** (*continued*).

be used to determine the number of sources in a basin and their respective stratigraphic and regional distribution, source age, lithology, depositional environment (marine, non-marine, lacustrine) and maturity [6]. Areas with overlapping petroleum systems can be identified in relation to possible oil mixing from two or more sources. Mapping source-related oil families enables clearer identification to predict the lateral

**Table 1**
Subsurface and surface oil samples.

| Oil field | Subsurface sample |
|---|---|
| Ku–Maloob–Zaap | KMZ1 |
| Ku–Maloob–Zaap | KMZ2 |
| Ku–Maloob–Zaap | KMZ3 |
| Ku–Maloob–Zaap | KMZ4 |
| Ku–Maloob–Zaap | KMZ5 |
| Cantarell | CAN1 |
| Cantarell | CAN2 |
| Cantarell | CAN3 |
| Cantarell | CAN4 |
| Cantarell | CAN5 |
| Cantarell | CAN6 |
| Cantarell | CAN7 |
| Cantarell | CAN8 |
| Cantarell | CAN9 |
| Cantarell | CAN10 |
| Cantarell | CAN11 |
| Cantarell | CAN12 |
| Cantarell | CAN13 |
| Cantarell | CAN14 |
| Cantarell | CAN15 |
| **Oil field** | **Surface sample** |
| Cantarell | EXD1 |
| Cantarell | EXD2 |
| Cantarell | EXD3 |
| Cantarell | EXD4 |

extent of oilfields and regional oil quality variation in different parts of a basin.

Here, geochemical data from subsurface and surface oil samples have been integrated using statistical analysis to discriminate the Cantarell oil seep origin. This is the first time the subsurface provenance of this major seepage area has been determined.

## 2. Material and methods

### 2.1. Geological setting

The site in the Akal Pillar province (Fig. 1A) on the Campeche State continental shelf constitutes the largest petroleum province in the Gulf of Mexico. The Cantarell seepage occurs primarily in shallow water areas of salt tectonics and active petroleum generation from Tithonian (Upper Jurassic) age source rocks, where faults and salt diapirs penetrate overlying sediments and create migration pathways, either from the source rock or reservoir, to the sea floor. The province is the "Villahermosa Uplift" offshore extension, which lies between the Comalcalco and Macuspana offshore basins. The Yucatán Platform slope zone defines its northeastern limit. Salt tectonics played an important role in defining the structural framework of major oilfields such as Cantarell. Thrust faults oriented in a northwest–southeast direction are the main Cantarell region structural features. They are associated with northwest–southeast trending folds, asymmetric or overturned to the northeast [4].

The studied site is the Pimienta–Tamabra petroleum system in the southern Gulf of Mexico, with 66.3 billion barrels of oil cumulative production and total reserves. The system's effectiveness is largely due to the widespread distribution of a good to excellent mature, Upper Jurassic source rock underlying numerous stratigraphic and structural traps that contain excellent carbonate reservoirs. The oil and gas expulsion as a supercritical fluid occurred when the overburden rock thickness exceeded 5 km. This burial event started in the Eocene, culminated in the Miocene, and continues to a lesser extent today. The expelled hydrocarbons started migrating laterally and then upward as gas-saturated 35–40 API gravity oil with a 500–1000 $ft^3$/barrels gas-to-oil ratio (GOR). The generation-accumulation efficiency is ca. 6% [7].

The source rocks giving rise to the Jurassic and Cretaceous oils are associated with marine carbonate environments. In contrast, those

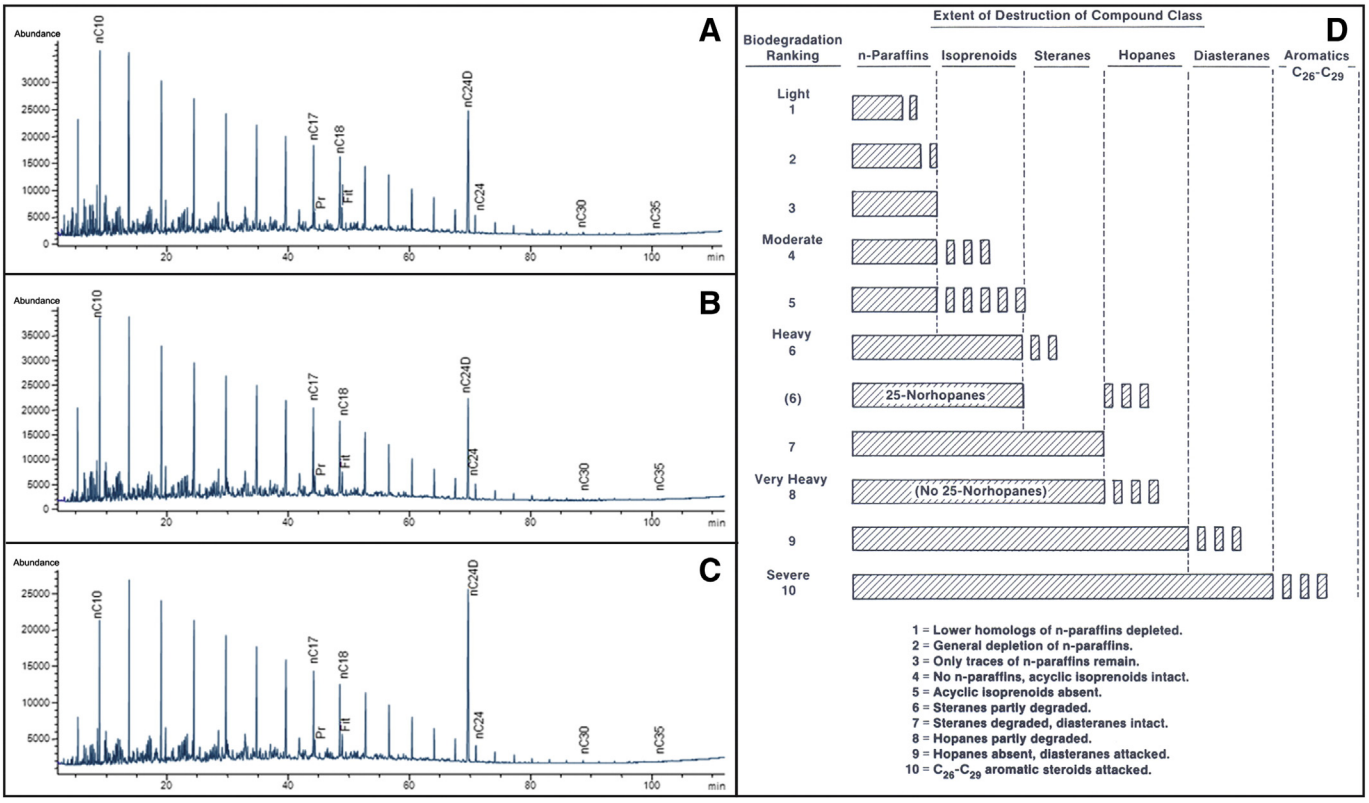


**Fig. 2.** GC-FID chromatograms of whole oil samples: (A) KMZ2, (B) KMZ5, (C) CAN9, $C_{24}$ D: internal standard, (D) biodegradation ranking a scale of 1 to 10 (1 lightly biodegradated to 10 severely biodegradated), Peters & Moldowan, 1993 [6].

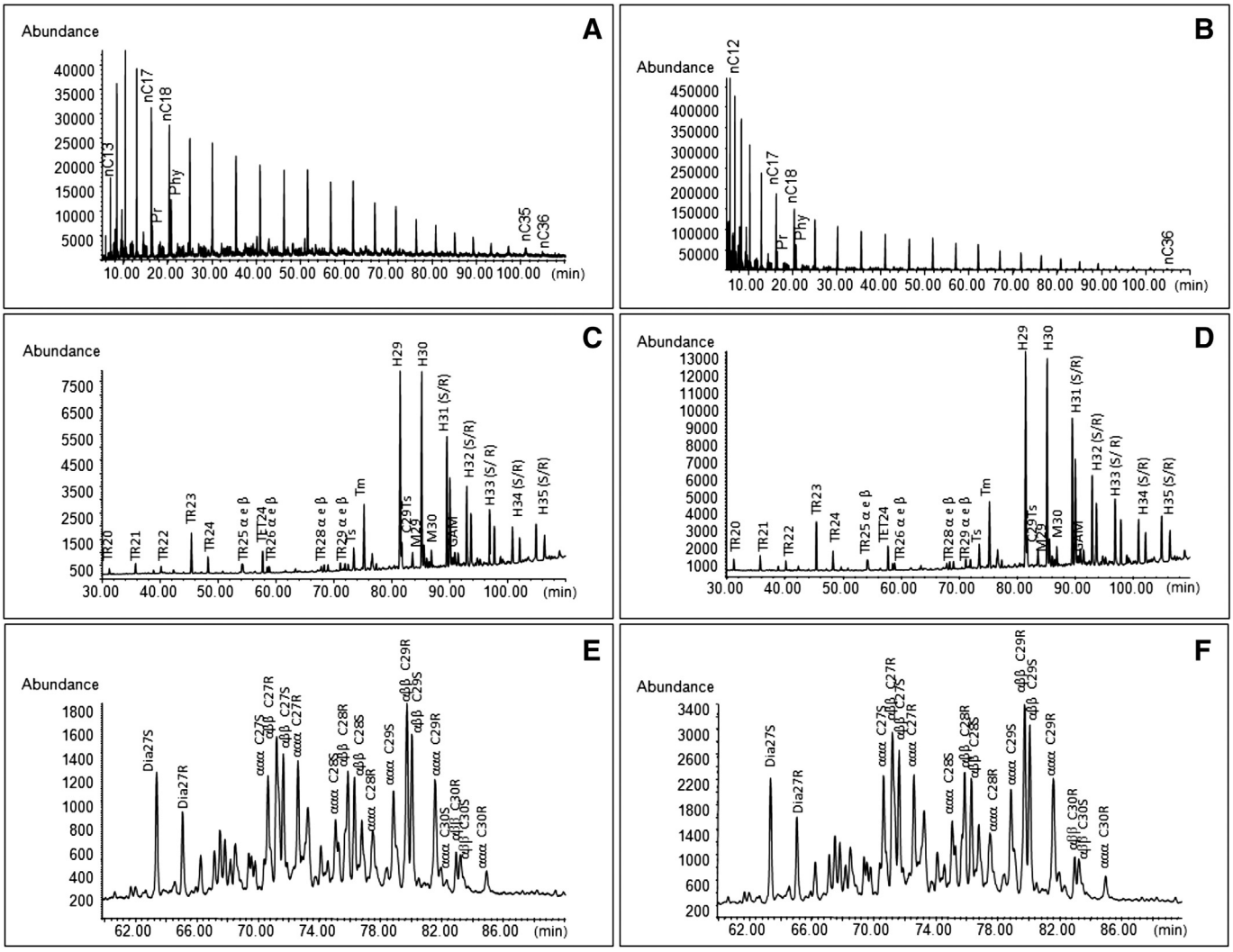


**Fig. 3.** Mass chromatograms: *m/z* 85 (A and B), *m/z* 191 (C and D) and *m/z* 217 (E and F) showing *n*-alkanes, terpanes and steranes' distribution, respectively. Fig. 3A, C and E from surface oil sample (seepage — EXD 3) and Fig. 3B, D and F from subsurface oil sample (CAN 9).

giving rise to the Tertiary oils are associated with a marine deltaic siliciclastic depositional setting. Biomarker and isotope differences in the oils derived from marine carbonate environments can be interpreted in terms of variation in salinity, clay content and oxygen depletion. The differences provide diagnostic criteria to recognize and differentiate four distinct organic-rich depositional regimes as the sources for the oil types: an anoxic hypersaline marine carbonate environment associated with a narrow and shallow semi-restricted sea (Oxfordian); an anoxic marine carbonate environment (Tithonian) and an anoxic marine evaporitic environment (Early Cretaceous); the Tertiary oils are derived from a bacterially reworked terrigenous and marine source deposited in a marine deltaic environment [8].

### 2.2. Samples

Twenty subsurface oil samples from the shelf and 4 oil seepage samples (Fig. 1A, B and Table 1) from Ku–Maloob–Zaap and Cantarell, situated in Akal Pillar (Fig. 1A), were analyzed. Seepage samples were collected in Cantarell area. It is characterized by a scenario where currents are not important (Fig. 1C) [9]. Taking into account the geology of the area, it was included in the map of Gulf of Mexico identifying structural geologic of the sampling site (Fig. 1D).

### 2.3. Sampling

#### 2.3.1. Surface oil (oil seeps)

The sampling employs a simple system which is passed through the oil to collect the sample. The system is then removed from the disposable ring/handle and placed in a glass jar with a cap for storage and transportation [10].

#### 2.3.2. Subsurface oil (oil from shelf)

Oil samples from different continental shelf locations were provided by PEMEX Exploración y Producción, Región Marina Norest (PEP/RMNE), Estudios Ambientales, México.

### 2.4. GC/flame ionization detection (GC-FID)

The samples were prepared for analysis by weighing ca. 10 mg oil in 1 mL dichloromethane (DCM). Whole oil analysis was carried out using a 5890 gas chromatograph equipped with a splitless injector and HP5-MS column, Hewlett-Packard Agilent Technologies, USA; (30 m × 0.25 mm i.d., 0.25 μm thickness film). $H_2$ was used as the carrier gas. The column temperature was programmed from 40 to

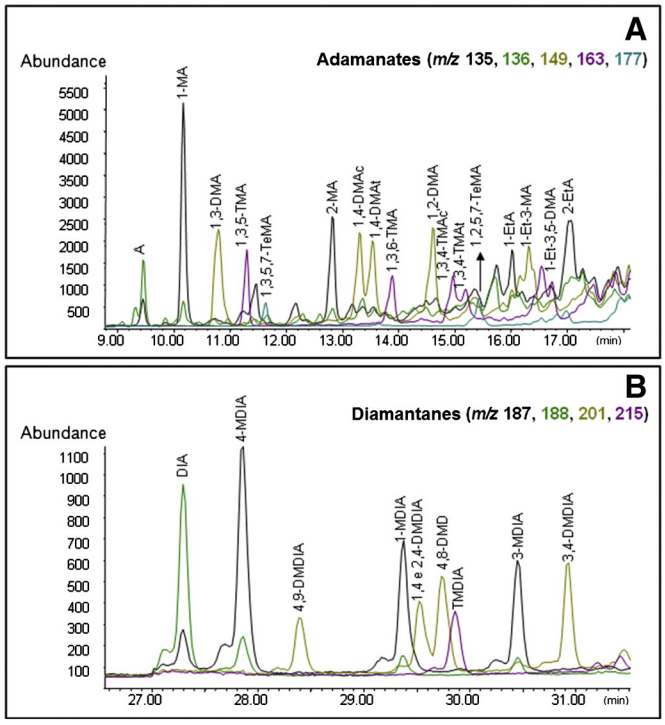


**Fig. 4.** Representative chromatograms for subsurface oil samples (CAN 6): (A) adamantanes: m/z 135, 136, 149, 163, 177; (B) diamantanes: m/z 187, 188, 201, 215.

320 °C at 2.5 °C·min$^{-1}$; injection volumes were of 1 μL, and detector temperature was 340 °C [11–13].

### 2.5. Sample separation

Liquid chromatography with an activated silica gel column was used [11]. Saturated hydrocarbon fractions were eluted with hexane, aromatic hydrocarbons with hexane:DCM (8:2) and NSO fractions with DCM: MeOH (9:1) [12,13]. Only saturated hydrocarbon fractions were used to analyze biomarkers and diamondoids.

### 2.6. GC-MS

GC-MS was used to obtain biomarker and diamondoid signatures from saturate fractions with an Agilent Technologies 6890 gas chromatograph equipped with a HP-5MS column (30 m × 0.25 mm i.d., 0.25 μm film thickness) coupled to an Agilent Technologies 5973 mass selective detector. The carrier gas was He and the injector temperature 280 °C. The mass spectrometer was operated in electron ionization mode at 70 eV [11–17].

#### 2.6.1. Biomarker analysis

Biomarkers analysis was performed from 55 to 150 °C at 20 °C·min$^{-1}$, then to 320 °C at 1.5 °C·min$^{-1}$. The injection volume was 1 μL in splitless mode. Data acquisition was carried out in select ion monitoring (SIM) mode. Regular steranes were examined using *m/z* 217 and *m/z* 218 mass chromatograms, while terpanes (mainly hopanes) were examined using *m/z* 191. Compounds were assigned by comparison of mass spectra and relative retention times with literature data [12,13].

#### 2.6.2. Diamondoid analysis

The samples were analyzed immediately after the liquid chromatography step to avoid possible evaporative loss. Diamondoid analysis was performed from 40° to 180 °C at 3 °C min$^{-1}$, then to 310 °C (held 10 min) at 6 °C min$^{-1}$. Injection volume was 2 μL in split mode (5:1). Data acquisition was performed in select ion monitoring (SIM) mode. Diamondoids were monitored using *m/z* 135, 136, 149 and 163 (adamantanes), and *m/z* 187, 188 and 201 (diamantanes). Compounds were assigned by comparison of mass spectra and relative retention times with literature data [13].

### 2.7. Data desk statistics program

Data from subsurface and surface oil samples were submitted to multivariate statistical analysis especially cluster analysis. All source parameters already described were analyzed using Euclidean distance as a clustering metric and the Ward's aggregation method.

## 3. Results and discussion

Subsurface and surface oil samples showed very similar composition but different ratios of biomarker and correlation parameters such as maturity and source. The criterions used to select the surface samples were that the seep is a permanent phenomenon in the Cantarell oil field and oil samples from the seep slick were collected concurrently with the acquisition of RADARSAT images. Subsurface oil samples were obtained from part of the oil field operation.

GC-FID analysis showed (Fig. 2A, B and C) homologous series of *n*-alkanes ranging from $C_9$ to $C_{35}$ and isoprenoids pristane ($C_{19}$) and phytane ($C_{20}$) which characterized the oils as very slightly biodegraded (Fig. 2D). Subsurface and surface oil samples showed similar distributions of biomarkers (Fig. 3) and diamondoids (Fig. 4). Mass chromatograms for *m/z* 85 showed (Fig. 3A and B) homologous series of *n*-alkanes ranging from $C_{12}$ to $C_{36}$ and isoprenoids pristane ($C_{19}$) and phytane ($C_{20}$). This property was corroborated by the absence of 25-s from all the *m/z* 191 mass chromatograms and by the preservation of hopanes (Fig. 3C and D) and steranes (Fig. 3E and F) in the *m/z* 191 and *m/z* 217 mass chromatograms, respectively. However, *m/z* 85 mass chromatograms from surface oil samples (Fig. 3A) showed a lower abundance of *n*-alkanes with low molecular weight vs. subsurface oil samples (Fig. 3B). Therefore, seepage samples showed volatile compounds ranging from *n*-$C_{12}$ to *n* $C_{15}$ volatilized due to various processes that alter crude oil in the marine environment, including spreading, aggregation, dispersion, evaporation and emulsification [6]. Many weathering mechanisms can alter the composition of oil while it migrates toward the surface. These include evaporation of the more volatile hydrocarbons and consumption by microorganisms [18].

Biomarker peak areas were integrated and maturity parameters such as $C_{30}$ moretane/$C_{30}$ hopane ($M_{30}/H_{30}$), 22S/22S + 22R $H_{32}$, 20S/(20S + 20R) $C_{29}$ ααα and ββ/(ββ + αα) $C_{29}$ steranes were obtained to evaluate the maturity degree. Plots of 22S/22S + 22R $H_{32}$ and ββ/ββ + αα $C_{29}$ vs. 20S/20S + 20R $C_{29}$ (Fig. 5A, B) for the $C_{29}$ steranes are particularly effective for describing oil maturity [12,13]. Most samples showed 22S/22S + 22R $H_{32}$ and 20S/20S + 20R $C_{29}$ ααα values plotting at the top of Fig. 5, indicating mature samples. KMZ4, KMZ5 and CAN2 samples were the exception and had values for 22S/22S + 22R $H_{32}$ slightly below these values. It was possible to observe that all samples showed ββ/ββ + αα $C_{29}$ values below the values in the cross plot of 20S/20S + 20R $C_{29}$ ααα vs. ββ/ββ + αα $C_{29}$ (Table 2). According to these characteristics, the oils may be classified as mature.

The moretanes (i.e.; 17β, 21α (H)) are less thermally stable than the 17α,21β(H)-hopanes, so an increase in maturity is followed by a decrease of moretane abundance relative to the corresponding hopanes. The $M_{30}/H_{30}$ ratio had values between 0.09 and 0.11 for all the oil samples (Table 2). These values led to the assumption that all were mature [6,19,20]. Samples showed high values of vitrinite reflectance equivalent, varying from 0.91 to 1.02. Therefore, the results indicated that the oils were from the peak of the oil generation window.

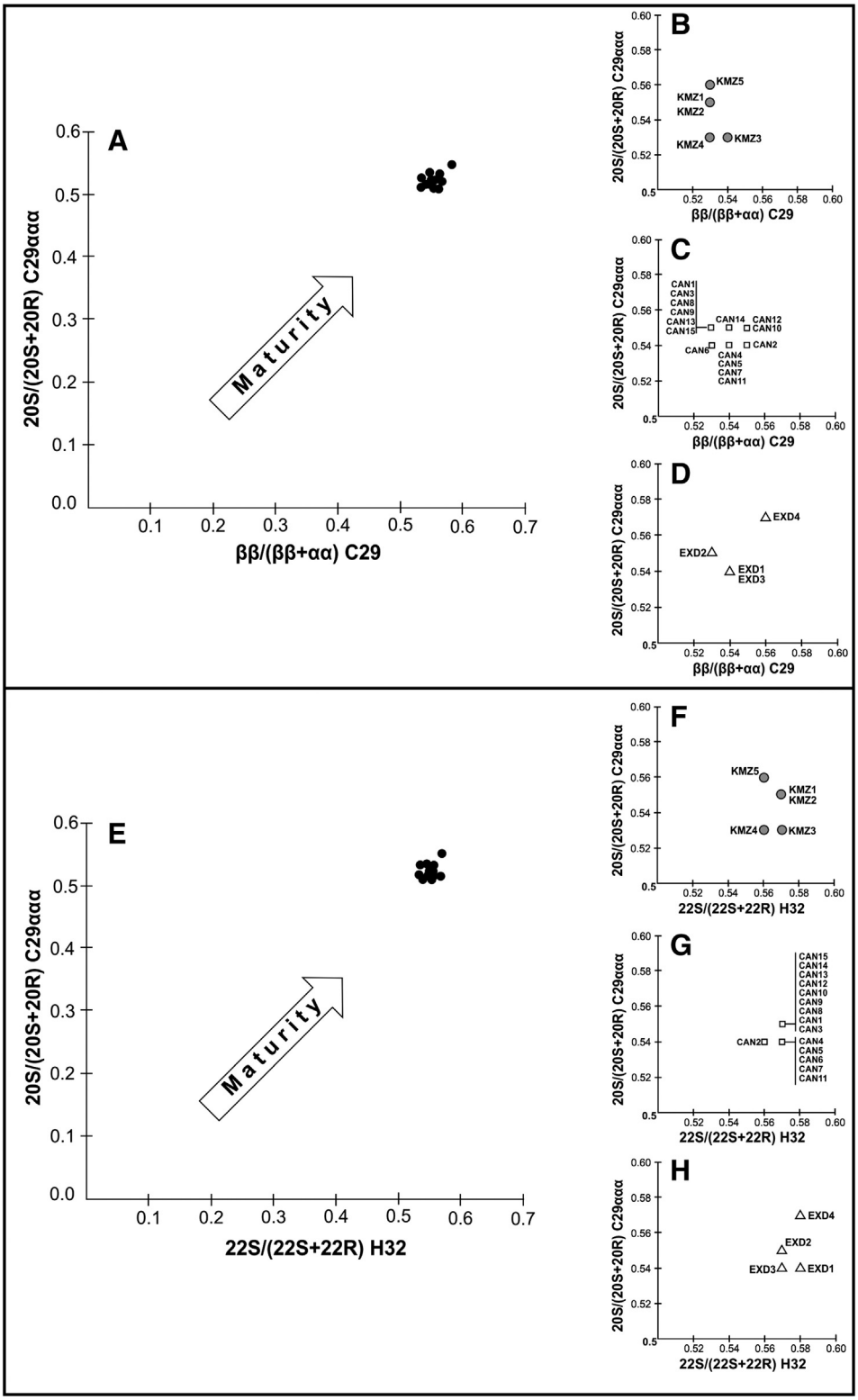


**Fig. 5.** Correlation between (A) ββ/ββ + αα C29 (all samples), (B) KMZ samples, (C) CAN samples, (D) EXD samples, (E) 22S/22S + 22R H32 versus 20S/20S + 20R C29 (all samples), (F) KMZ samples, (G) CAN samples (H) EXD samples for maturity parameters.

Biomarker and diamondoid peak areas were integrated and source parameters such as $C_{27}$-18α(H)-trisnorhopane/$C_{27}$-17α(H)-trisnorhopane (Ts/Tm), $C_{27}$–$C_{28}$–$C_{29}$ regular steranes, $H_{29}/H_{30}$, $H_{35}/H_{34}$ and relative abundance of 3,4-dimethyldiamantane (3,4-DMD), 4,8-dimethyldiamantane (4,8-DMD) and 4,9-dimethyldiamantane (4,9-DMD) were obtained to evaluate source type.

No sample reached the maximum Ts/Tm value; the highest value being 0.42 for sample KMZ5, well below the maximum [6,21]. All the

**Table 2**
Biomarker parameters for maturity evaluation.

| Sample | 22S/(22S + 22R) $H_{32}$[a] | 20S/(20S + 20R) $C_{29}\alpha\alpha\alpha$[b] | ββ/(ββ + αα) $C_{29}$[c] | $M_{30}/H_{30}$[d] | Ro equivalent[e] |
|---|---|---|---|---|---|
| KMZ1 | 0.57 | 0.55 | 0.53 | 0.10 | 0.95 |
| KMZ2 | 0.57 | 0.55 | 0.53 | 0.11 | 0.95 |
| KMZ3 | 0.57 | 0.53 | 0.54 | 0.10 | 0.91 |
| KMZ4 | 0.56 | 0.53 | 0.53 | 0.09 | 0.91 |
| KMZ5 | 0.56 | 0.56 | 0.53 | 0.11 | 0.98 |
| CAN1 | 0.57 | 0.55 | 0.53 | 0.10 | 0.96 |
| CAN2 | 0.56 | 0.54 | 0.55 | 0.10 | 0.95 |
| CAN3 | 0.57 | 0.55 | 0.53 | 0.10 | 0.97 |
| CAN4 | 0.57 | 0.54 | 0.54 | 0.09 | 0.93 |
| CAN5 | 0.57 | 0.54 | 0.54 | 0.09 | 0.95 |
| CAN6 | 0.57 | 0.54 | 0.53 | 0.10 | 0.93 |
| CAN7 | 0.57 | 0.54 | 0.54 | 0.10 | 0.95 |
| CAN8 | 0.57 | 0.55 | 0.53 | 0.09 | 0.95 |
| CAN9 | 0.57 | 0.55 | 0.53 | 0.10 | 0.97 |
| CAN10 | 0.57 | 0.55 | 0.55 | 0.09 | 0.96 |
| CAN11 | 0.57 | 0.54 | 0.54 | 0.09 | 0.95 |
| CAN12 | 0.57 | 0.55 | 0.55 | 0.10 | 0.96 |
| CAN13 | 0.57 | 0.55 | 0.53 | 0.10 | 0.96 |
| CAN14 | 0.57 | 0.55 | 0.54 | 0.10 | 0.96 |
| CAN15 | 0.57 | 0.55 | 0.53 | 0.10 | 0.95 |
| EXD1 | 0.58 | 0.54 | 0.54 | 0.10 | 0.95 |
| EXD2 | 0.57 | 0.55 | 0.53 | 0.10 | 0.96 |
| EXD3 | 0.57 | 0.54 | 0.54 | 0.09 | 0.94 |
| EXD4 | 0.58 | 0.57 | 0.56 | 0.09 | 1.02 |

[a] 17α, 21β(H)-30-bishomohopane $C_{32}$ 22S/(17α, 21β(H)-30-bishomohopane $C_{32}$ 22S + 17α, 21β(H)-30-bishomohopane $C_{32}$ 22R) (*m/z* 191).
[b] 20S/(20S + 20R) 5α, 14α, 17α(H), 24-ethylcholestane (*m/z* 217).
[c] (20S + 20R) 5α, 14β, 17β(H), 24-ethylcholestane/((20S + 20R) 5α, 14β, 17β(H), 24-ethylcholestane + (20S + 20R) 5α, 14α, 17α(H), 24-ethylcholestane (*m/z* 217).
[d] 17β, 21α(H)-hopane (moretane) $C_{30}$/17α, 21β(H)–hopane $C_{30}$ (*m/z* 191).
[e] ½(20S C29ααα/20R C29ααα) + 0.35 (*m/z* 217).

**Table 3**
Biomarker parameters for source evaluation.

| Amostra | $Tr_{24}/Tr_{21}$[a] | $Tr_{26}/Tr_{25}$[b] | $Tet_{24}/H_{30}$[c] | Ts/Tm[d] | $H_{29}/H_{30}$[e] | Hop/Est[f] | $H_{34}/H_{35}$[g] | $H_{35}/H_{34}$[h] | $\%C_{27}\alpha\beta\beta$[i] | $\%C_{28}\alpha\beta\beta$[j] | $\%C_{29}\alpha\beta\beta$[l] | Gam/$H_{30}$[m] |
|---|---|---|---|---|---|---|---|---|---|---|---|---|
| KMZ1 | 1.37 | 0.79 | 0.11 | 0.36 | 1.09 | 1.59 | 0.92 | 1.09 | 34.87 | 28.93 | 36.20 | 0.12 |
| KMZ2 | 1.38 | 0.75 | 0.11 | 0.35 | 1.08 | 1.55 | 0.9 | 1.11 | 34.93 | 28.80 | 36.27 | 0.12 |
| KMZ3 | 1.37 | 0.89 | 0.11 | 0.36 | 1.07 | 1.71 | 0.87 | 1.15 | 35.83 | 28.65 | 35.52 | 0.12 |
| KMZ4 | 1.28 | 0.79 | 0.08 | 0.32 | 1.01 | 1.86 | 0.85 | 1.18 | 32.51 | 27.96 | 39.53 | 0.12 |
| KMZ5 | 1.41 | 0.81 | 0.10 | 0.42 | 1.03 | 1.36 | 0.88 | 1.14 | 36.32 | 28.79 | 34.90 | 0.12 |
| CAN1 | 1.35 | 0.79 | 0.11 | 0.39 | 1.01 | 1.69 | 0.89 | 1.12 | 32.97 | 28.99 | 38.06 | 0.11 |
| CAN2 | 1.29 | 0.83 | 0.12 | 0.38 | 1.02 | 1.59 | 0.87 | 1.15 | 36.19 | 28.66 | 35.15 | 0.11 |
| CAN3 | 1.21 | 0.87 | 0.13 | 0.38 | 1.03 | 1.59 | 0.88 | 1.14 | 35.45 | 28.73 | 35.82 | 0.11 |
| CAN4 | 1.38 | 0.86 | 0.11 | 0.38 | 1.01 | 1.81 | 0.88 | 1.14 | 35.68 | 28.38 | 35.94 | 0.12 |
| CAN5 | 1.31 | 0.87 | 0.11 | 0.38 | 1.02 | 1.56 | 0.89 | 1.12 | 34.48 | 28.79 | 36.73 | 0.11 |
| CAN6 | 1.34 | 0.86 | 0.11 | 0.38 | 1.03 | 1.65 | 0.87 | 1.15 | 34.28 | 28.56 | 37.16 | 0.11 |
| CAN7 | 1.28 | 0.85 | 0.12 | 0.38 | 1.02 | 1.57 | 0.87 | 1.15 | 34.80 | 28.74 | 36.46 | 0.10 |
| CAN8 | 1.42 | 0.90 | 0.12 | 0.39 | 1.04 | 1.73 | 0.91 | 1.1 | 35.01 | 28.83 | 36.16 | 0.11 |
| CAN9 | 1.28 | 0.83 | 0.12 | 0.38 | 1.03 | 1.55 | 0.89 | 1.12 | 36.75 | 25.48 | 37.77 | 0.10 |
| CAN10 | 1.27 | 0.83 | 0.12 | 0.38 | 1.03 | 1.67 | 0.88 | 1.14 | 35.43 | 28.49 | 36.08 | 0.11 |
| CAN11 | 1.30 | 0.86 | 0.12 | 0.38 | 1.03 | 1.70 | 0.88 | 1.14 | 35.96 | 28.51 | 35.53 | 0.11 |
| CAN12 | 1.21 | 0.81 | 0.12 | 0.38 | 1.03 | 1.82 | 0.88 | 1.14 | 36.80 | 26.35 | 36.85 | 0.12 |
| CAN13 | 1.29 | 0.90 | 0.12 | 0.38 | 1.03 | 1.59 | 0.88 | 1.14 | 34.69 | 28.87 | 36.44 | 0.11 |
| CAN14 | 1.31 | 0.89 | 0.12 | 0.38 | 1.02 | 1.56 | 0.89 | 1.12 | 34.86 | 28.59 | 36.55 | 0.12 |
| CAN15 | 1.27 | 0.94 | 0.12 | 0.37 | 1.03 | 1.58 | 0.89 | 1.12 | 34.73 | 28.60 | 36.67 | 0.12 |
| EXD1 | 1.57 | 0.91 | 0.11 | 0.38 | 1.02 | 1.76 | 0.91 | 1.1 | 33.87 | 28.76 | 37.37 | 0.11 |
| EXD2 | 1.62 | 0.91 | 0.12 | 0.39 | 1.03 | 1.73 | 0.89 | 1.12 | 34.59 | 29.13 | 36.28 | 0.11 |
| EXD3 | 1.63 | 0.87 | 0.11 | 0.39 | 1.04 | 1.97 | 0.91 | 1.1 | 35.63 | 28.57 | 35.81 | 0.11 |
| EXD4 | 1.71 | 0.88 | 0.11 | 0.39 | 1.04 | 2.20 | 0.94 | 1.06 | 33.38 | 27.60 | 39.03 | 0.10 |

[a] $Tr_{24}/Tr_{21}$: Terpane tricyclic $C_{24}$/Terpane tricyclic $C_{21}$ (*m/z* 191).
[b] $Tr_{26}/Tr_{25}$: Terpane tricyclic $C_{26}$/Terpane tricyclic $C_{25}$ (*m/z* 191).
[c] $Tet_{24}/H_{30}$: Terpane tetracyclic $C_{24}$/17α (H), 21β(H)–hopane $C_{30}$ (*m/z* 191).
[d] Ts/Tm: 18α(H)-22,29,30-trisnorneohopane $C_{27}$/17α(H)-22,29,30-trisnorhopane ($C_{27}$) (*m/z* 191).
[e] $H_{29}/H_{30}$: 17α (H), 21β(H)–30-norhopane $C_{29}$/17α (H), 21β(H)–hopane $C_{30}$ (*m/z* 191).
[f] Hop/Est: ($H_{29}$–$H_{33}$)/[$C_{27}$, $C_{28}$, $C_{29}$ ααα (20S + 20R) + $C_{27}$, $C_{28}$, $C_{29}$ αββ (20S + 20R)] (*m/z* 191 e *m/z* 217).
[g] $H_{34}/H_{35}$: 17α (H), 21β(H)-30,31,32,33-tetrakishomohopane $C_{34}$ 22 (S + R)/17α (H), 21β(H)-30,31,32,33,34-pentakishomohopane $C_{35}$ 22 (S + R) (*m/z* 191).
[h] $H_{35}/H_{34}$: 17α (H), 21β(H)-30,31,32,33,34-pentakishomohopano $C_{35}$ 22 (S + R)/17α (H), 21β(H)-30,31,32,33-tetrakishomohopane $C_{34}$ 22 (S + R) (*m/z* 191).
[i] $\%C_{27}\alpha\beta\beta$: [$C_{27}\alpha\beta\beta$ / ($C_{27}\alpha\beta\beta$ + $C_{28}\alpha\beta\beta$ + $C_{29}\alpha\beta\beta$)] * 100 (*m/z* 217).
[j] $\%C_{28}\alpha\beta\beta$: [$C_{28}\alpha\beta\beta$ / ($C_{27}\alpha\beta\beta$ + $C_{28}\alpha\beta\beta$ + $C_{29}\alpha\beta\beta$)] * 100 (*m/z* 217).
[l] $\%C_{29}\alpha\beta\beta$: [$C_{29}\alpha\beta\beta$ / ($C_{27}\alpha\beta\beta$ + $C_{28}\alpha\beta\beta$ + $C_{29}\alpha\beta\beta$)] * 100 (*m/z* 217).
[m] Gam/$Hop_{30}$: Gammacerene/17α (H), 21β(H)–hopane $C_{30}$ (*m/z* 191).

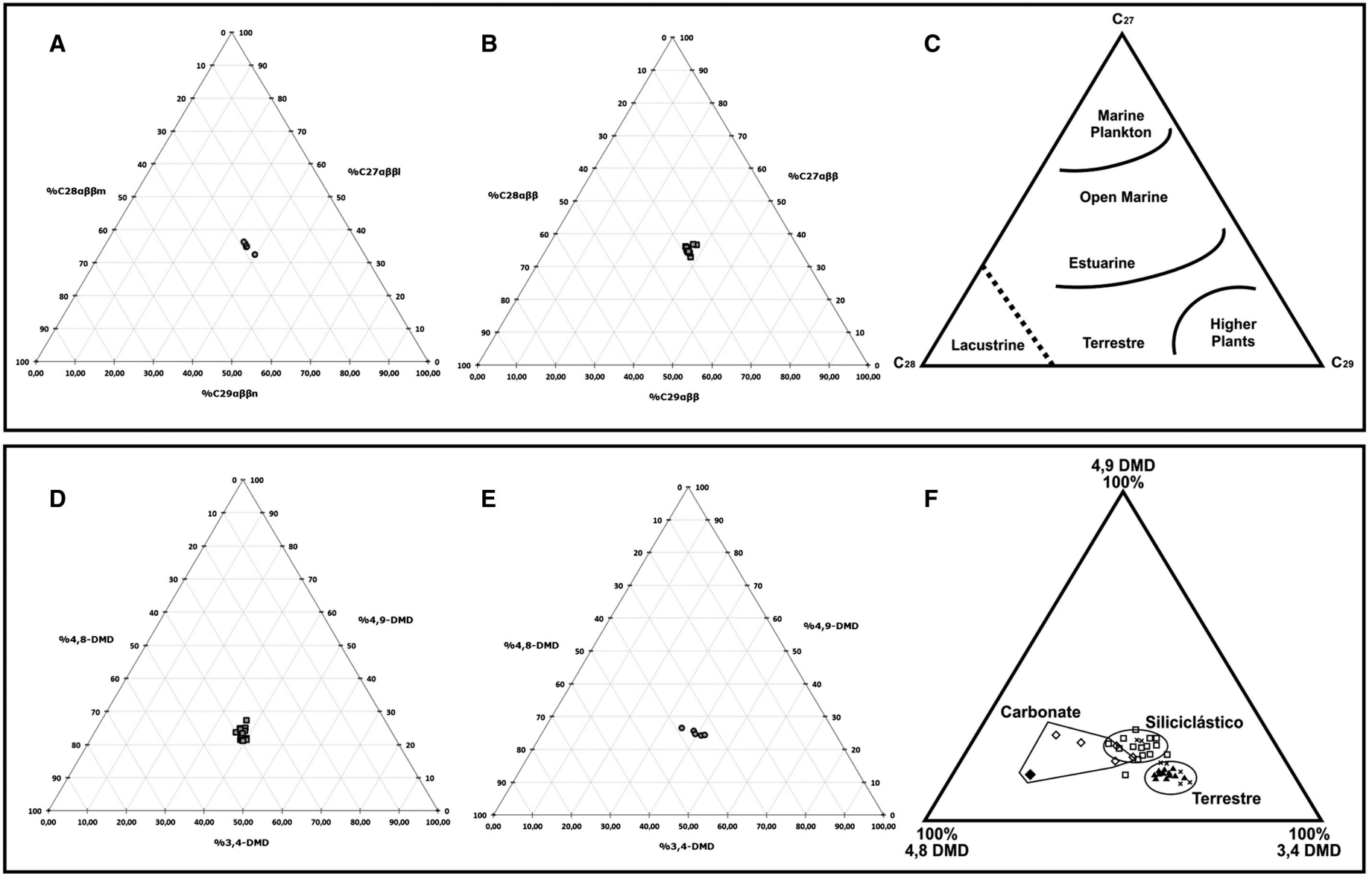


**Fig. 6.** Ternary diagrams showing (A) relative abundances of $C_{27}$, $C_{28}$ and $C_{29}$ regular steranes (KMZ) (B) Relative abundances of $C_{27}$, $C_{28}$ and $C_{29}$ regular steranes (CAN) (C) relative abundances of $C_{27}$, $C_{28}$ and $C_{29}$ regular steranes [Huang and Meinschein (1979)] (D) relative abundance of 3,4-, 4,8- and 4,9- dimethyladamantanes for source parameters (KMZ), (E) relative abundance of 3,4-, 4,8- and 4,9- dimethyladamantanes for source parameters (CAN), (F) relative abundance of 3,4-, 4.8- and 4,9-dimethyladamantanes for source parameters (Schultz et al., 2001).

oils had values <1, i.e. between 0.32 and 0.42 (Table 3). Values less than unity are associated with a marine carbonate depositional environment [11].

Although the samples in general had a similar relative abundance of $C_{27}$ and $C_{29}$ regular steranes close to each other the $C_{29}$ regular steranes were relatively more abundant, indicating a terrestrial contribution (Table 3). KMZ3, KMZ5, CAN2 and CAN11 oil samples showed a relative abundance of $C_{27}$ regular steranes higher than $C_{28}$ and $C_{29}$ regular steranes, indicating marine phytoplankton (Table 3). The relative distributions of $C_{27}$, $C_{28}$ and $C_{29}$ regular steranes were plotted in a ternary diagram (Fig. 6A and B) to distinguish organic matter type. The oils are seen to be related (Fig. 6C), being derived from an open marine or estuarine source rock from comparison with [22].

High values for $H_{29}/H_{30}$ (>0.6), combined with high values for $H_{35}/H_{34}$ (>0.8) are common for oils from marine carbonate source rocks (Peters et al., 2005), so these values of $H_{29}/H_{30}$ from 1.01 to 1.09 and $H_{35}/H_{34}$ from 1.06 to 1.18 (Table 3) are in agreement with a marine carbonate depositional environment.

Hopane/sterane (Hop/Ste) ratios showed low values, ranging from 1.36 to 2.20 (Table 3). As values for this ratio ≤4 indicate marine organic matter input, while values >7 indicate terrestrial organic matter input [23,24], this ratio also corroborates a marine organic matter input.

The relative abundances of 3.4-DMD, 4.8-DMD and 4.9-DMD (Table 4) were plotted on a ternary diagram (Fig. 6D and E) that indicates oils showing an abundance of 3.4-DMD and 4.8-DMD near to and higher than 4.9-DMD, respectively, suggesting that the samples were situated in a mixed region that can be derived from a carbonate and/or siliciclastic organic matter type according to [25] (Fig. 6F).

All samples showed very similar saturated hydrocarbon distributions, probably indicating that the oils had essentially the same origin. Previous studies [8] demonstrated that geochemical analysis could classify the oils from the Mexican part of the Gulf into four families related by age and source rock depositional environment (Fig. 7 A). Oils that belong to family 1 were associated with an anoxic hypersaline marine carbonate environment (Oxfordian), family 2 with an anoxic marine carbonate environment (Tithonian), family 3 with an anoxic marine evaporitic environment (Early Cretaceous) and family 4 to a marine deltaic environment (Tertiary). The correlation of $H_{35}/H_{34}$ vs. $H_{29}/H_{30}$ was used to characterize age and source rock depositional environment for the studied oils. All the samples belong to family 2 (Fig. 7B and Table 3), indicating an origin from marine source rocks of Tithonian age. According to [7,8]; Tithonian oils are related to a carbonate source rock deposited under anoxic/suboxic conditions. Therefore, this study's results corroborate the depositional environment and the source rock's age.

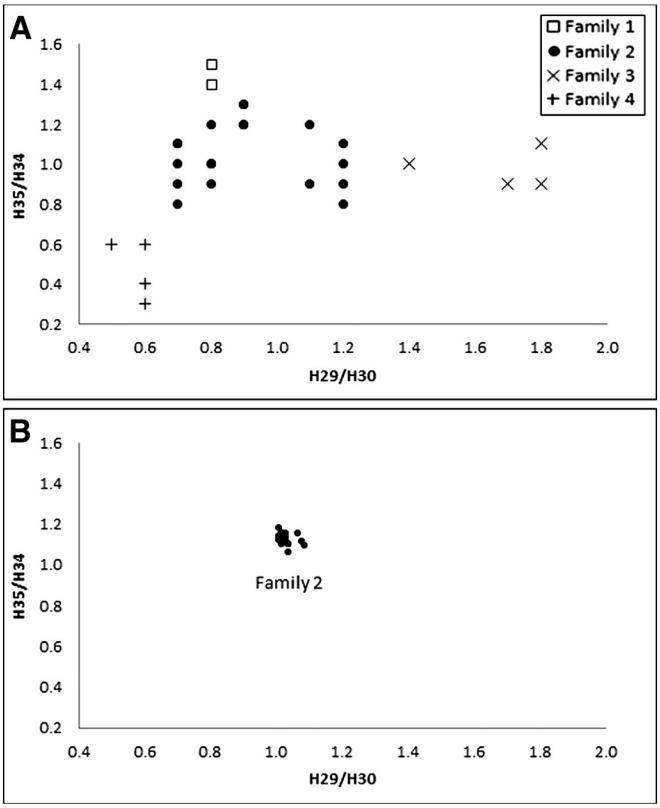


**Fig. 7.** (A) Oil families from the Gulf of Mexico (adapted from Guzman-Vèga and Mello, 1999). (B) Correlations between $H_{35}/H_{34}$ vs. $H_{29}/H_{30}$ for the analyzed oil samples.

In spite of being generated from the same source rock, small differences in geochemical parameters (biomarkers and diamondoids) were observed between oils produced by different rigs from the selected reservoir. These are due to organic facies variability, thermal evolution and migration.

Hierarchical cluster analysis is an important tool that groups samples according to their similarities. Within the same group, samples have the greatest similarities while between groups they have the lowest similarities [26]. Source parameters were provided (Table 3) for hierarchical cluster analysis. Averages (Fig. 8) for each of the clusters were included. From Fig. 8 and analysis of variance, it can be affirmed

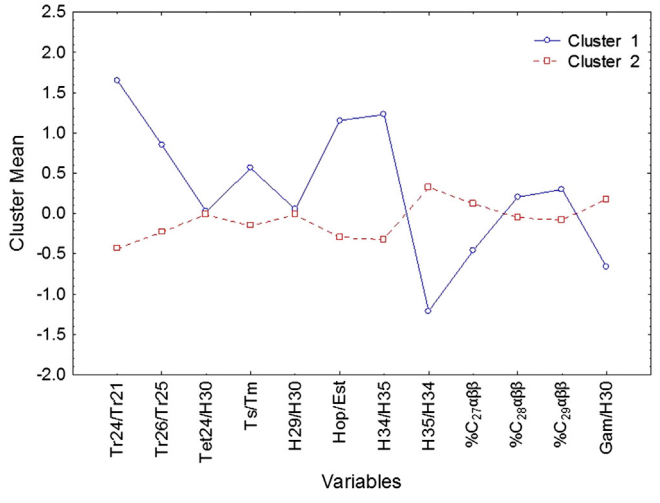


**Fig. 8.** Cluster mean as a function of the variables.

**Table 4**
Relative abundance (%) of 3,4-dimethyldiamantane (3,4-DMD), 4,8-dimethyldiamantane (4,8-DMD) and 4,9-dimethyldiamantane (4,9-DMD).

| Sample | 4,9-DMD | 4,8-DMD | 3,4-DMD |
|---|---|---|---|
| KMZ1 | 24.3 | 34.6 | 41.1 |
| KMZ2 | 25.7 | 35.8 | 38.6 |
| KMZ3 | 24.8 | 35.9 | 39.3 |
| KMZ4 | 24.4 | 33.7 | 42.0 |
| KMZ5 | 26.6 | 38.4 | 34.9 |
| CAN1 | 25.0 | 38.4 | 36.7 |
| CAN2 | 23.7 | 40.0 | 36.3 |
| CAN3 | 21.9 | 38.2 | 39.9 |
| CAN4 | 21.4 | 40.0 | 38.6 |
| CAN5 | 24.5 | 38.5 | 37.0 |
| CAN6 | 27.4 | 35.5 | 37.2 |
| CAN7 | 25.0 | 36.9 | 38.1 |
| CAN8 | 21.7 | 39.0 | 39.3 |
| CAN9 | 22.3 | 39.4 | 38.2 |
| CAN10 | 24.2 | 37.4 | 38.3 |
| CAN11 | 24.7 | 38.4 | 36.9 |
| CAN12 | 21.5 | 38.5 | 40.0 |
| CAN13 | 21.3 | 39.7 | 39.0 |
| CAN14 | 21.1 | 39.5 | 39.4 |
| CAN15 | 23.4 | 38.4 | 38.1 |

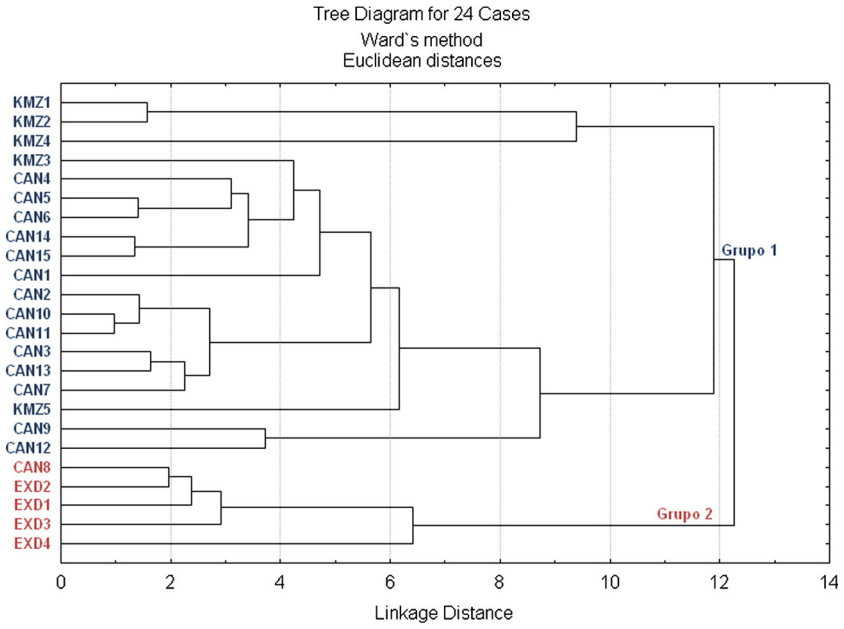


**Fig. 9.** Dendrogram of hierarchical cluster analysis for subsurface and surface (seepage) oil samples.

that variables $Tr_{24}/Tr_{21}$, $Tr_{26}/Tr_{25}$, Hop/Est, $H_{34}/H_{35}$, $H_{35}/H_{34}$ discriminate the clusters. These variables represent good correlation observed between the geochemical analysis of the seep oil samples (EXD1 to EXD4) and a unique subsurface oil sample CAN8 from the Paleocene–Cretaceous breccia reservoir (Fig. 9). The seep correlation with a specific petroleum reservoir suggests that the seep origin is from this reservoir, and not from the source rock.

## 4. Conclusions

Geochemical analysis shows that surface and subsurface oil samples are very similar, indicating the same origin (source rock). Based on the correlation of $H_{35}/H_{34}$ vs. $H_{29}/H_{30}$, it was possible to indicate that the oils were from marine source rocks of Tithonian age. Mass chromatograms of *m/z* 85 and *m/z* 191 showed the presence of *n*-alkane distribution and the absence of 25-norhopanes, respectively. This indicates that the oils were not biodegraded. However, surface oil samples had a higher level of biodegradation than subsurface ones. All samples showed relative abundances of $C_{27}$ to $C_{29}$ regular steranes and of 3,4-, 4,8- and 4,9-DMD as with marine source rocks deposited under anoxic conditions. Therefore, the biomarker ratios as 22S/22S + 22R $H_{32}$ and ββ/ββ + αα $C_{29}$ vs. 20S/20S + 20R $C_{29}$ indicated that the oils stem from mature oil reservoirs. Diamondoid data were used as a source parameter and corroborated the biomarker analyses.

Fingerprinting data were used not only to characterize the samples and conduct a diagnostic study of the affected area, but also to characterize and identify the seep oil sources. Despite the similarities, small differences could be observed and facilitated the correlation studies between the samples. Cluster analysis indicated a good correlation of the seepage samples with a unique subsurface oil sample, CAN8, from the reservoir in the Paleocene/Cretaceous breccia. Seepage in the Cantarell oil field is most probably fed by the geologic reservoir (Paleocene/Cretaceous breccia) rather than by the Tithonian source rock.

## Acknowledgments

The authors wish to thank PEMEX Exploración y Producción (PEP) for their generous support in the preparation of the study and for permission to publish the final results. We also thank Dr[a] Veronica Calado (UFRJ-EQ) for support in statistic analysis.

## References

[1] C.J. Wendt, A. Cyphers, How the Olmed used bitumen in ancient Mesoamerica, J. Anthropol. Archaeol. 27 (2) (2008) 175–191.
[2] T.H. Naehr, D. Birgel, G. Bohrmann, I.R. MacDonald, S. Kasten, Biogeochemical controls on authigenic carbonate formation at the chapopote "asphalt volcano", Bay of Campeche, Chem. Geol. 266 (2009) 390–402.
[3] Petróleos Mexicanos (Pemex), Los reservas de Hidrocarburos de México, Los principales campos de petróleo y gas de México, vol. 2, Pemex Exploración y Producción, México, 1999.
[4] F.P. Miranda, A.M.Q. Marmol, E.C. Pedroso, C.H. Beisl, P. Welgan, L.M. Morales, Analysis of RADARSAT-1 data for offshore monitoring activities in the Cantarell Complex, Gulf of Mexico, using the unsupervised semivariogram textural classifier (USTC), Can. J. Remote. Sens. 30 (2004) 424–436.
[5] A. Mendoza, F.P. Miranda, K. Bannerman, E. Pedroso, O. López, M. Herrera, Satellite environmental monitoring of oil spills in the south Gulf of Mexico, Offshore Technology Conference, Houston, Texas, 2004.
[6] K.E. Peters, J.M. Moldowan, The Biomarker Guide, Interpreting Molecular Fossils in Petroleum and Ancient Sediments, second ed. Prentice Hall, Englewood Cliffs, New Jersey, 1993.
[7] L.B. Magoon, T.L. Hudson, H.E. Cook, Pimienta-Tamabra(!) — A giant supercharged petroleum system in the southern Gulf of Mexico, onshore and offshore Mexico, in: C. Bartolini, R.T. Buffler, A. Cantú-Chapa (Eds.), The western Gulf of Mexico Basin: Tectonics, Sedimentary Basins, and Petroleum Systems, Am. Assoc. Pet. Geol. Mem., 75, 2001, pp. 83–125.
[8] M.A. Guzmán-Vega, M.R. Mello, Origin of oil in the Sureste Basin, Mexico, Am. Assoc. Pet. Geol. Bull. 83 (1999) 1068–1095.
[9] National Oceanic and Atmospheric Administration, Flower Garden Banks, a Regional Context, Currents, 2014, http://flowergarden.noaa.gov/about/naturalsetting.html#currents .
[10] ASTM (American Society for Testing, Materials, Reapproved 2006), Annual Book of ASTM Standards, Sampling Practices for Sampling of Waterborne Oil, Methods D 4489-95. W. Conshohocken, PA, USA, 1995.
[11] K. Grice, R. Alexander, R.I. Kagi, Diamondoid hydrocarbon ratios as indicators of biodegradation in Australian crude oils, Org. Geochem. 31 (2000) 67–73.
[12] D.A. Azevedo, J.B. Tamanqueira, J.C.M. Dias, A.P.B. Carmo, F.T.T. Gonçalves, L. Landau, Multivariate statistical analysis of diamondoid and biomarker data in selected oil samples from Brazilian basins, Fuel (Guildford) 87 (2008) 2122–2130.
[13] M.V. Springer, D.F. Garcia, F.T.T. Gonçalves, L. Landau, D.A. Azevedo, Diamandoid and biomarker characterization of oils from the Llanos Orientales Basin, Colombia, Org. Geochem. 41 (2010) 1013–1018.
[14] D.A. Azevedo, J.B. Tamanqueira, J.C.M. Dias, A.P.B. Carmo, L. Landau, F.T.T. Gonçalves, Multivariate statistical analysis of diamondoid and biomarker data from Brazilian basin oil samples, Fuel 87 (2008) 2122–2130.
[15] A. Permanyer, D.A. Azevedo, F.T.T. Goncalves, Characterization of Brazilian oils by FTIR and SUVF spectroscopy. A comparison with GC/MS results, Geogaceta 38 (2005) 139–141.
[16] J.R. Heckmann, R. Pereira, F.T.T. Gonçalves, L. Landau, D.A. Azevedo, Avaliação geoquímica de óleos Brasileiros com ênfase nos hidrocarbonetos aromáticos, Quím. Nova 34 (2011) 1328–1333.
[17] G. Kadir, R.T. Simoneit, B. Zühtü, İ.H. Karamanderesi, V. Baki, Origin of petroliferous bitumen from the Büyük Menderes–Gediz geothermal graben system, Denizli–Sarayköy, western Turkey, Appl. Geochem. 22 (7) (2007) 1393–1415.

[18] J.M. Hunt, Petroleum Geochemistry and Geology, second ed. Freeman, New York, 1996.
[19] A.S. Mackenzie, J.M.E. Quirke, J.R. Maxwell, Molecular parameters of maturation in the Toarcian shales, Paris basin, France-I. Changes in the configuration of acyclic isoprenoid alkanes, steranes and triterpanes, Geochim. Cosmochim. Acta 44 (1980) 1709–1721.
[20] W.K. Seifert, J.M. Moldowan, The effect of thermal stress on source rock quality as measured by hopane stereochemistry, Phys. Chem. Earth 12 (1980) 229–237.
[21] A.R. Rabbani, M.R. Kamali, Source rock evaluation and petroleum geochemistry offshore SW Iran, J. Pet. Geol. 28 (2005) 413–428.
[22] W.Y. Huang, W.G. Meinschein, Sterols as ecological indicators, Geochim. Cosmochim. Acta 43 (1979) 739–745.
[23] M.R. Mello, P.C. Gaglianone, S.C. Brassell, J.R. Maxwell, Geochemical and biological marker assessment of depositional environments using Brazilian offshore oils, Mar. Pet. Geol. 5 (1988) 205–223.
[24] M.R. Mello, N. Telnaes, P.C. Gaglianone, M.I. Chicarelli, S.C. Brassell, J.R. Maxwell, Organic geochemical characterization of depositional palaeoenvironments of source rocks and oils in Brazilian marginal basins, Org. Geochem. 13 (1988) 31–45.
[25] L.K. Schulz, A. Wilhelms, E. Rein, R.A. Steen, Application of diamondoids to distinguish source rock facies, Org. Geochem. 32 (2001) 365–375.
[26] J.M. Moita Neto, G.C. Moita, Uma introdução a análise exploratória de dados multivariados, Quím. Nova 20 (1998) 467–469.